Intrinsic properties of a Burridge-Knopoff model of an earthquake fault

J. M. Carlson
Department of Physics, University of California, Santa Barbara, California 93106

J. S. Langer, B. E. Shaw, and C. Tang
Institute for Theoretical Physics, University of California, Santa Barbara, California 93106
(Received 26 December 1990)

We present a detailed numerical study of certain fundamental aspects of a one-dimensional homogeneous, deterministic Burridge-Knopoff model. The model is described by a massive wave equation, in which the key nonlinearity is associated with the stick-slip velocity-weakening friction force at the interface between tectonic plates. In this paper, we present results for the statistical distribution of slipping events in the limit of a very long fault and infinitesimally slow driving rates. Typically, we find that the magnitude distribution of smaller events is consistent with the Gutenberg-Richter law, while the larger events occur in excess of this distribution. The crossover from smaller to larger events is identified with a correlation length describing the transition from localized to delocalized events. We also find that there is a sharp upper cutoff describing the maximum large event. We identify how the correlation length and this upper cutoff scale with the parameters in the model. We find that both are independent of system size, while both do depend on the spatial discretization. In addition to the magnitude distribution, we present a series of measurements of other seismologically relevant quantities, including the event duration, the size of the rupture zone, and the energy release, and discuss the relationship between our measurements and the corresponding empirical laws in seismology.

I. INTRODUCTION

We have reported recently [1–4] that a simple, purely deterministic version of the Burridge-Knopoff model [5] of an earthquake fault behaves in ways that seems at least qualitatively similar to what is observed in nature. In particular, for seismic events of small or moderately large sizes, the distribution of events $\mathcal{N}(\mu)$ of magnitude μ produced by this model is consistent with the Gutenberg-Richter law,

$$\mathcal{N}=Ae^{-b\mu}\ , \tag{1.1}$$

where A is a constant and $b\approx 1$, yet rises appreciably higher at the upper end of the spectrum where most of the seismic energy is released [6].

While the model is clearly too simple in several important respects—its strict uniformity, its one-dimensionality, its lack of a mechanism for producing aftershocks, etc.—this simplicity makes it particularly useful as a paradigm for a real earthquake fault. We build into it no extrinsic stochastic ingredients, no complex structure, and effectively only two dimensionless groups of system-dependent parameters. Thus we can be fairly sure that the rich variety of behavior patterns that emerges is intrinsic to this general class of dynamical systems and not some artifact of special features. It therefore makes sense to use this model to suggest questions that we might ask about real seismological data.

Accordingly, the purpose of the investigation reported here has been to explore, primarily by numerical means, some features of the artificial catalogs of seismic events that can be generated by this model. We pay special attention to those features which—at least in principle—can be measured for real faults: the seismic moments of events, their spatial extents, their durations, the energy released, etc. Our advantage is that these artificial catalogs span the equivalent of hundreds of thousands of years on real faults, with perfect efficiency of detection across the entire spectrum of magnitudes. Thus, unlike observational seismologists, we can measure the frequency distributions for very large events, and we even can ask about the limiting distributions describing infinitely long faults and infinitesimally small loading rates.

In Secs. II and III of this paper, we review the basic dynamical features of this model, introducing two technical changes that we have found convenient primarily for computational efficiency. The frequency distributions and their scaling properties are described in Sec. IV. Section V is devoted to a discussion of various other seismologically interesting features of the events. We conclude with a discussion of our results in Sec. VI. In the Appendix we summarize certain aspects of the relationship between the Richter scale and other seismological measurement scales, and the relationship between these measurements, and the measurements we make numerically.

II. DYNAMICAL FEATURES OF THE MODEL

As discussed in Ref. [2], our version of the Burridge-Knopoff model is defined by a partial-differential equation of the form

$$\ddot{U}=\xi^2\frac{\partial^2 U}{\partial s^2}-U-\phi(2\alpha v+2\alpha\dot{U})\ , \tag{2.1}$$

where $U(s,\tau)$ is the displacement relative to equilibrium on one side of the fault; on the other side the plate is

moving at a relative velocity v. Here $U(s,\tau)$ is a function of position along the fault s and a dimensionless time τ measured in units of a characteristic slipping period that, for real faults, is roughly of order seconds or less [7]. The displacement U correspondingly is measured in units of a characteristic slipping distance, roughly of order meters. Dots denote derivatives of U with respect to τ.

Apart from the nonlinear dissipative term ϕ, which we shall discuss in the next paragraph, (2.1) is a linear, massive wave equation; that is, a Klein-Gordon equation. The mass, i.e., the coefficient of $-U$ on the right-hand side of (2.1) is unity because of our choice of units of time; this term is a measure of the shearing stresses which tend to keep the points on either side of the fault aligned with the positions of the countermoving tectonic plates. The term $\xi^2\partial^2 U/\partial s^2$ is the acceleration due to longitudinal (compressional) stresses along the fault.

We find it convenient to keep the position s as a dimensional variable with units of length; thus the stiffness length ξ in (2.1) is wave speed multiplied by the characteristic slipping time and therefore is of the order of a kilometer or so. Throughout all of this discussion, we shall be describing numerical integrations of the finite-difference version of (2.1):

$$\ddot{U}_i = l^2(U_{i+1}+U_{i-1}-2U_i)-U_i-\phi(2\alpha v+2\alpha\dot{U}_i)\ , \tag{2.2}$$

where $l=\xi/a$ and a is the grid spacing—in the language of the original Burridge-Knopoff model, the equilibrium spacing between the blocks. [For convenience, the elements in the finite-difference approximation (2.2) will be referred to as "blocks," but this term need not be taken literally.] The length a, which never appears explicitly in any calculations, is the ultraviolet cutoff for the model. Because ξ is a finite, physically meaningful length, the continuum limit $a\to 0$ is equivalent to letting the dimensionless parameter $l=\xi/a$ become infinite. For real faults, the ultraviolet cutoff a may be associated with a smoothing length arising from a stable creep component of the friction law at very small velocities (see Ref. [2]), the details of which may vary somewhat for different faults. However, if realistic sizes for the smallest events that can be thought of as "earthquakes" are of the order of tens of meters [8], then the natural value for the dimensionless parameter l is of order 10^2. Thus it appears that the continuum limit might be a good approximation. We shall not be able to use so fine a mesh size in our simulations, but we shall see that such a large dynamic range is not necessary in order to understand the basic features of this model. We shall also see, however, that some important properties of the model are sensitive to the ultraviolet cutoff.

The function ϕ appearing in (2.1) and (2.2) is the velocity-dependent "stick-slip" friction law shown in Fig. 1. The quantity v that appears in its argument is the loading speed in units of the slipping speed and, accordingly, is of order 10^{-8} or smaller. The quantity α is the ratio of the slipping speed to the speed at which the friction law decreases to half of the magnitude that it had at threshold. We expect both of these speeds to be of about the same magnitude; thus α is of order unity. Note that larger values of α mean weaker slipping friction and more-pronounced instability.

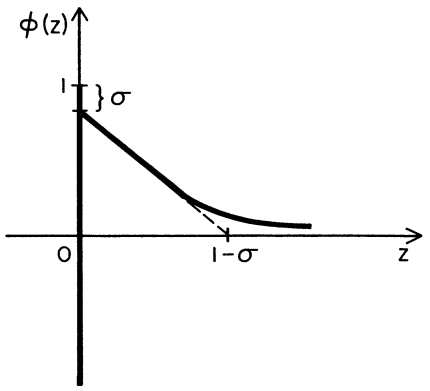

FIG. 1. The slip-stick friction law, defined in Eq. (2.5). Sticking friction $\phi(0)$ satisfies $\phi(0)\le 1$, while slipping friction decays monotonically to zero from the initial value $\phi(0^+)=1-\sigma$ with initial slope equal to -1. Note that the forms of Eq. (2.1) and (2.2) are invariant (upon resetting the zero of displacement) with respect to addition of a constant to the high-speed friction.

The conventional measure of the size of a seismic event is the "moment," which we define to be

$$M=a\sum_{i\ \mathcal{E}}\delta U_i\approx\int_{\mathcal{E}}\delta U(s)ds\ , \tag{2.3}$$

where the δU_i are the total displacements of the connected set of blocks that move during an event $\mathcal{E}$. The corresponding "magnitude" μ is

$$\mu=\ln\left[\frac{M}{m}\right]\ , \tag{2.4}$$

where m has the units of moment, and determines the zero of the magnitude scale. (We shall use $m=a$, the ultraviolet cutoff, and take $a=1$ in all of our numerical calculations.) In the Appendix we shall make some remarks about the relationship between our definitions of M and μ and those used in the seismological literature.

We have made two changes from our previous definition of ϕ. First, the sticking friction at zero relative velocity can have any value in the range $(-\infty,1]$, as opposed to being symmetric about $\phi=0$ with the range $[-1,1]$ as previously defined. This means that we allow no backward motions; that is, $\dot{U}\ge -v$ always, which is most likely a realistic assumption. A realistic slipping friction probably does not vanish at high velocities as in Fig. 1. Rather, it is more likely to approach some nonzero constant or, perhaps, pass through a minimum and start rising again at high speeds. Because all other terms in (2.1) or (2.2) are linear, we can shift the zero of ϕ by shifting the zero of U; thus the ϕ shown in Fig. 1 can be an accurate approximation for a friction law in which the force at finite velocities decreases by only a small fraction of its maximum value at threshold.

The second change shown in Fig. 1 is more important. Note that, while the sticking threshold remains at unity

(in dimensionless units), slipping friction begins at $\phi=1-\sigma$. Throughout the work described here, we have used

$$\phi(z)=\begin{cases}(-\infty,1], & z=0\\ (1-\sigma)/\{1+[z/(1-\sigma)]\}, & z>0\ .\end{cases} \tag{2.5}$$

The effect of this modification is that slipping events start abruptly with acceleration $\ddot{U}$ proportional to σ instead of gradually with the third derivative $\dddot{U}$ proportional to v, as is the case when $\sigma=0$. The advantage is that the individual events are no longer controlled in any way by the loading speed v, which we can now assume to be arbitrarily small. In fact, for vanishingly small v, independent slipping events never overlap in time. One can therefore integrate (2.2) forward in time with $v=0$ until all blocks have come to rest, and then simply scan the system to find the block for which the forces are closest to threshold, thereby identifying the position and time of the next slipping event. This simplification of the computational procedure has permitted us to extend the calculations reported here to larger systems than we had been able to deal with before.

III. LOCALIZED AND DELOCALIZED EVENTS

In our previous analysis, we found that there was an important distinction, both statistically and dynamically, between the smaller "localized" events and the larger "delocalized" events. The crossover was roughly associated with events of a particular size $\tilde{\xi}$, which could be estimated analytically, and was found to diverge in the limit as $v\to 0$. Here an important consequence of our modified friction law is that σ replaces v as the critical parameter in the system. That is, it is σ rather than v which enters into the length $\tilde{\xi}$. Because $\tilde{\xi}$ is conceptually very important in our analysis, it will be useful to rederive an expression for this quantity before proceeding to an analysis of numerical results.

First, for an event in which only a single block slips, the solution of (2.2) is

$$\delta U(\tau)\cong\frac{\sigma}{\omega_1^2}(1-\cos\omega_1\tau)\ , \tag{3.1}$$

where

$$\omega_1^2=2l^2+1\ . \tag{3.2}$$

Here $\delta U(\tau)$ is the net displacement relative to the initial position at which the block became unstuck. (We assume that l is large enough that we can neglect the $\dot{U}$ dependence of ϕ here.) The total displacement in this event is

$$M_1\equiv a\ \delta U\left[\frac{\pi}{\omega_1}\right]=\frac{2\sigma a}{\omega_1^2}\ , \tag{3.3}$$

and the maximum speed attained is σ/ω_1.

Now consider a region of size Δs in which all of the blocks are near the threshold of slipping. This means that in the continuum limit

$$\xi^2\frac{d^2U_\epsilon}{ds^2}-U_\epsilon\cong 1,\quad U_\epsilon\cong -1+\epsilon\cosh(s/\xi) \tag{3.4}$$

where ϵ is some constant. As in Ref. [2], we write $U(s,\tau)=U_\epsilon(s)+\delta U(s,\tau)$, linearize (2.1) in δU, and find a solution of the form

$$\delta\dot{U}(s,\tau)\cong\frac{\sigma\xi}{2\omega_1^2}e^{\alpha\tau}[\delta(s-s_0-\xi\tau)+\delta(s-s_0+\xi\tau)] \tag{3.5}$$

for the case in which σ is very small and the large event is triggered by a one-block event at $s=s_0$, $\tau=0$. That is, in its early stage, this idealized event consists of a pair of narrow pulses, propagating outward from an epicenter at s_0 with speed ξ, and growing exponentially as they move. We call Δs the triggering zone, because initially the system is on the verge of slipping in this region. Consequently, as the pulses propagate through this region, they gain kinetic energy.

In order for the event to remain localized, the pulses must remain sufficiently small so that they cannot propagate far into the more firmly stuck regions at the boundary of the triggering zone [9]. Roughly speaking, this condition will be met if the displacements δU, which are generated by the pulses at the edges of the triggering zone, are small enough (less than a number of order unity) so that they cannot transfer sufficient strain to the boundary to exceed the slipping threshold there. Assuming that the event begins near the center of the region, so that each pulse moves a distance of order $\Delta s/2$ through the triggering zone, and because a pulse takes a time $\Delta\tau=\Delta s/2\xi$ to move a distance $\Delta s/2$, the localization condition becomes

$$2\xi\,\Delta\tau=\Delta s<\tilde{\xi}\equiv\frac{2\xi}{\alpha}\ln\left[\frac{4l^2}{\sigma}\right]\ . \tag{3.6}$$

If we take Eq. (3.5) literally as a complete description of a marginally localized event of size $\tilde{\xi}$, then the moment associated with the event would be

$$\tilde{M}=\int\delta\dot{U}\,ds\,d\tau\cong\frac{2\xi}{\alpha}\ . \tag{3.7}$$

In fact, the linear approximation used in the derivation of (3.5) is not likely to be valid for the entire event. The propagating pulses will not die immediately upon reaching the edges of the triggering zone, but are likely to be reflected back into the zone and decay as they propagate some distance into the stuck region at the boundary. The most we can say with confidence is that $\tilde{M}$ should scale like ξ, and that it will also depend in some way on α. However, for clarity in what follows, we shall adopt (3.7) as our definition of $\tilde{M}$.

While $\tilde{\xi}$ and $\tilde{M}$ are not defined or derived precisely by this analysis, they do set scales for this system that seem to capture quite accurately the most important physics of the crossover from localized to delocalized events. The exponential factor in (3.5), which describes the way in which the stored elastic energy is converted to kinetic energy in the early stages of a slipping event, tells us that the minimum size of a triggering zone in which a pulse can gather enough energy to break out and propagate through stuck regions must scale logarithmically with the triggering parameter σ (for $\sigma\ll 1$). The corresponding moment $\tilde{M}$ is independent of σ. For reasons noted in the

preceding paragraph, however, one should not conclude that the moment M generally scales exponentially with the size Δs. Complete events ordinarily do not consist of single pairs of pulses, nor do they remain in the regime where the linearized version of (2.1) is valid.

The dynamical role of $\tilde{\xi}$ as a localization length implies that it also serves as a correlation length for this system, albeit in a way that seems not particularly well suited for theoretical analysis. As discussed in Ref. [2], the underlying mechanism that produces chaotic behavior in this model is the instability associated with the velocity-weakening part of the friction law; irregularities in $U(s)$ are amplified during slipping events. More precisely, an event of size Δs amplifies local irregularities on length scales smaller than itself, but it smooths the system on larger scales. The piece of the system which is slipping is, on the average, catching up with its neighboring regions. Thus, localized events are actually smoothing the system—producing correlations—on scales less than or equal to $\tilde{\xi}$. Once a sufficiently smooth region is formed and reaches the slipping threshold, it triggers a large delocalized event which reestablishes the irregularities for another loading cycle, that is, for the next interval between large events.

From this point of view—which we believe to be correct, at least for this model—the events which comprise the small-events scaling region are not self-generated, but are simply the processes by which the chaotic configurations left by large events become smoother on small scales. Thus it appears that this model produces two separate and distinct classes of events, localized and delocalized, and that the dynamics of the delocalized events control the statistical distribution of the localized ones.

At present, we know relatively little about the dynamics of these large events other than what we can see in numerical experiments. We do not know enough about how they produce the localized events distribution to be able to predict the relevant exponents or amplitudes, nor can we compute from first principles the frequency distribution of these large events themselves. We turn next to an examination of the frequency distributions as deduced from numerical integration of (2.2).

IV. FREQUENCY DISTRIBUTIONS AND SCALING LAWS

As before, our procedure has been to start with some arbitrarily selected, nonuniform initial set of positions U_i and integrate (2.2) for hundreds (or thousands) of loading periods ν^{-1}. A typical sequence of events is shown in Fig. 2. Here we have plotted $U_i+\nu\tau$ as a function of $i=s/a$ in a series of consecutive fully "stuck" configurations. Because $\dot{U}_i=-\nu$ for blocks which are not slipping forward, stuck blocks remain stationary in this representation. The area between consecutive curves is the moment M of the event which has caused the displacement.

The distinction between localized and delocalized events shows up clearly in Fig. 2. By far the most numerous events are the small ones which occur in the local minima of $U(s)$. Equally obvious is the fact that the largest part of the area of the figure is covered by the much less frequent, delocalized events. It is also apparent that there are correlations between these events. The epicenters of the delocalized events nearly always occur near centers of small-scale activity. (See Ref. [4] for a detailed analysis of this effect.) Moreover, these epicenters themselves appear to occur in correlated sequences [10].

In Ref. [2], we defined $\mathcal{R}(\mu)d\mu$ to be the frequency of events, per unit length of the fault, with magnitudes in the interval between μ and $\mu+d\mu$. Here, however, because we take the limit of zero loading speed ν, it is more convenient to use the quantity $\mathcal{D}(\mu)\equiv\mathcal{R}(\mu)/\nu$ [or, in terms of moment rather than magnitude, $D(M)=R(M)/\nu$], which is the number of events per unit displacement instead of per unit time. The sum rule that states that the average displacement of the blocks must be the same as that of the plate to which they are attached now reads

$$\int M\mathcal{D}(\mu)d\mu=1 \ . \tag{4.1}$$

A set of magnitude-versus-frequency distributions

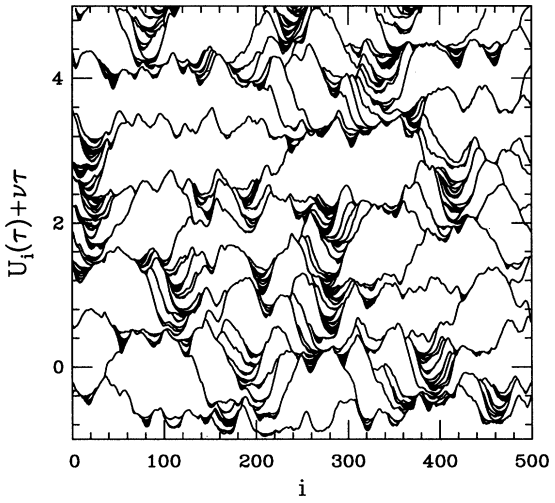

FIG. 2. Localized and delocalized events. A sequence of fully stuck configurations $U_i(\tau)+\nu\tau$ is shown as a function of position $i=s/a$ along the fault. There is a sharp distinction between the smaller, more abundant, localized events, which act mainly to smooth out the local minima in the configuration, and the larger delocalized events, in which the displacements are substantially larger, and which generate a net roughening of the system. The results shown here are for $N=500$, $\alpha=1.1$, $l=3$, and $\sigma=0.01$. At this value of α there is still a sharp distinction between localized and delocalized events, even though it is near the limit $\alpha=1$ where this distinction disappears in the magnitude-vs-frequency distribution (compare Figs. 3 and 6). For larger values of α the picture is similar, although the displacements associated with the small events are even smaller relative to the large events than they appear here. When $\alpha=1$, the picture is also similar, in the sense that the small events tend to cluster and there appear to be some correlations between the large events, though in that case the frequency distribution is described by a single power law.

$\mathcal{D}(\mu)$ for fixed α and three different values of l is shown in Fig. 3. These distributions exhibit the same characteristic features that we described in Refs. [1] and [2] for sufficiently large α: a broad "scaling region" for the smaller localized events, a pronounced peak for large, delocalized events, and a distinct minimum marking the crossover between the two regions. This minimum, which would correspond observationally to a gap in the seismic spectrum for a single fault, may be the physically most unrealistic aspect of this model. We believe that the gap is an artifact of the one dimensionality of the present version of the model, and plan to present evidence supporting this assertion in a future publication. The distinction between localized and delocalized events, however, and the associated fact that the frequency of delocalized events appreciably exceeds what one would predict by extrapolating $\mathcal{D}(\mu)$ from the scaling region, seems to be an intrinsic feature of this class of models, and also to be consistent with presently available seismological data.

The differential equation (2.1) is invariant under the transformation

$$\xi \to h\xi, \quad s \to hs \tag{4.2}$$

where h is an arbitrary constant. Because $M \to hM$ and $\mathcal{D}(\mu) \to \mathcal{D}(\mu)/h$ under this transformation, one might expect that $\mathcal{D}(\mu)$ would obey a scaling law of the form

$$\mathcal{D}(\mu) = \frac{1}{M} f(M/\xi) = \frac{1}{\xi} g(M/\xi) \ . \tag{4.3}$$

This scaling form would be consistent with our expectation that the crossover between localized and delocalized events occurs at $M \cong \tilde{M} \cong 2\xi/\alpha$, which scales linearly with ξ, and thus sets an appropriate scale for measuring M. To test this expectation, we have examined $\ln[\xi\mathcal{D}(\mu)]$ as a function of $\ln(M/\xi)$ for various values of l and (fixed) α. Our numerical results indicate that the quantity M/ξ is the correct independent variable in (4.3) for $M < \tilde{M}$ and large enough α; that is, for the region of localized events and for values of α such that the localization effect is well defined. (The small-α case is discussed separately below.) However, we find that the characteristic [11] (i.e., average) moment of the delocalized events does not scale like $\tilde{M}$ under any circumstances.

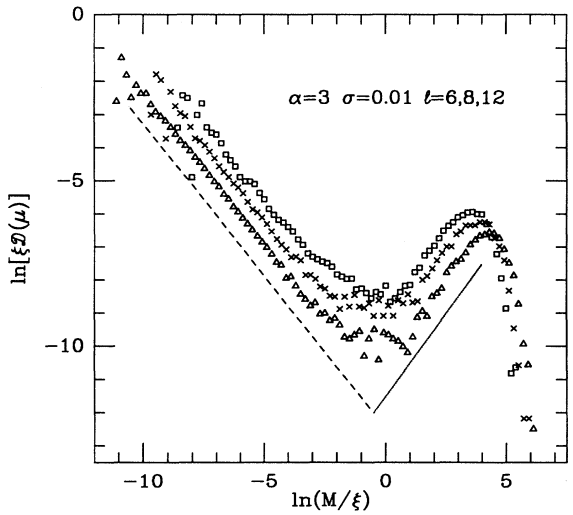

FIG. 3. The magnitude-vs-frequency distribution $\mathcal{D}(\mu)$, shown here for $l=6$, 8, and 12 and fixed $\alpha=3$. The system size is $N=4096$ for $l=6$ (squares) and 8 (crosses), while $N=8192$ for $l=12$ (triangles). In each case the sizes of the largest events are substantially smaller than the system size. The dashed line illustrates the slope of a least-squares fit to the scaling region, giving a value of $b=0.92$, while the dotted line with slope $-b'=1$ gives the slope of our best fit for the large events distribution. The fact that the minima coincide when we plot $\ln[\xi\mathcal{D}(\mu)]$ vs $\ln(M/\xi)$ is consistent with our expectation that the crossover from localized to delocalized events should occur at $M \approx \tilde{M} \propto \xi$. However, the failure of this scaling for the overall rate of events and the upper cutoff M^* illustrates the breakdown of the continuum scaling proposed in (4.3), and thus indicates that the ultraviolet cutoff a (through the explicit dependence on $l=\xi/a$) plays an important role in the model.

Figure 3 illustrates the l variation of the frequency distribution $\mathcal{D}(\mu)$ for a fairly large value of α. For each set of parameters $\tilde{\xi}$ is much less than N, thus the effects of system size should not be important. Indeed, in each case the value of N is large enough that even the biggest of the delocalized events never spans the whole system.

Several features of the distributions shown in Fig. 3 are especially important. First, the minima all occur at almost the same place, just below $\ln(M/\xi)=0$, in accord with our expectation that the crossover between localized and delocalized events occurs near $M=\tilde{M}$. Second, for $M < \tilde{M}$, each of the distributions has slope $-b$ with $b \approx 1$. Because the smallest events occur at $M = M_1 \approx \sigma a/l^2$, these distributions extend further to the left for larger values of l. However, as l increases at constant M/ξ, $\xi\mathcal{D}(\mu)$ decreases. Finally, the distributions of delocalized events, with $M > \tilde{M}$, rise almost linearly (note the dotted line with slope $-b'=1$) and then are cut off sharply at the l-dependent values of M that we shall denote M^*.

The above observations suggest the following approximations [3] for $\mathcal{D}(\mu)$:

$$\mathcal{D}(\mu) \approx \begin{cases} A(\tilde{M}/M)^b, & M_1 < M < \tilde{M} \\ A'(M/M^*)^{-b'}, & \tilde{M} < M < M^* \\ 0, & M < M_1,\ M^* < M \end{cases} \tag{4.4}$$

where $M^*/\tilde{M}$ is some function of l, and A and A' are constants to be determined. For the typical cases shown here, that is, for not-too-small α, the sum rule (4.1) is dominated by the large events with moments near M^*, and the localized events make a negligible contribution. From this observation it follows that

$$A' \approx (-b'+1)/M^* \ . \tag{4.5}$$

The condition that $\mathcal{D}(\mu)$ be continuous at $\tilde{M}$ is sufficient to determine the value of A:

$$A \approx \left[\frac{-b'+1}{M^*}\right]\left[\frac{\tilde{M}}{M^*}\right]^{-b'} \ . \tag{4.6}$$

The data shown in Fig. 3 are roughly consistent with a

relationship of the form $M^*/\tilde{M} \approx l^\gamma$, with $\gamma \approx 1$ for large α, and the value $b' \approx -1$ for the distribution of large events [12]. (We have not explored a large enough range of values of l to have verified the power-law behavior of $M^*/\tilde{M}$, and we certainly do not have an accurate estimate of the exponent γ. We report the results in this way simply to indicate the nature of the observed l dependence.) From these numerical input parameters and Eq. (4.6), it follows that $A \sim (\xi l^2)^{-1}$ and, from Eq. (4.5), that $A' \sim (\xi l)^{-1}$. Therefore, in accord with Eq. (4.4), we show in Fig. 4 that the distributions of localized events fall accurately on top of one another if we plot $\ln(\xi l^2 \mathcal{D})$ as a function of $\ln(M/\xi)$, and in Fig. 5 that the delocalized events scale properly if we plot $\ln(\xi l \mathcal{D})$ as a function of $\ln(M/\xi l)$. The fact that Eq. (4.4) has explicit l dependence means that the ultraviolet cutoff $a = \xi/l$ plays an important role.

Our results for the variations in the magnitude-versus-frequency distribution as the parameter l is increased allow us to extrapolate to relevant seismological ranges where $l \sim 100$. From this we can estimate the corresponding range in moment spanned by the localized and delocalized events on the seismological scale. In the model the localized events range from the lower cutoff M_1 up to $\tilde{M}$. Using Eqs. (3.3) and (3.7), and assuming that the l dependence dominates the scaling, we see that this corresponds to a magnitude range of about six decades (in seismology magnitude is measured with respect to a base-ten logarithm [13]):

$$\delta\mu_0 = \log_{10}\left[\frac{\tilde{M}}{M_1}\right] \sim \log_{10}\left[\frac{l^3}{\sigma}\right] \sim \log_{10}(l^3) \approx 6 \ . \tag{4.7}$$

On the other hand, for the large events, ranging for $\tilde{M}$ to

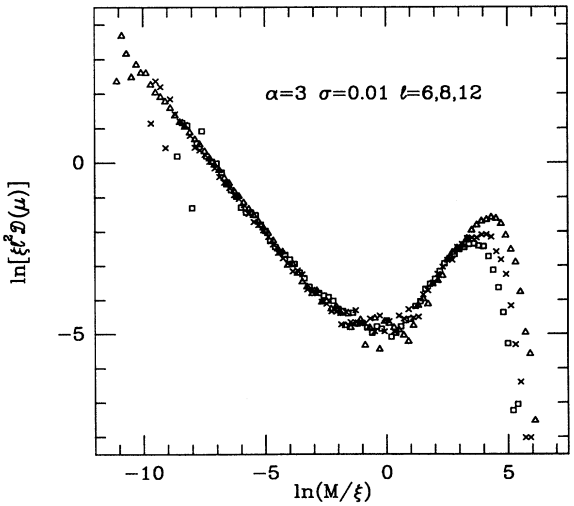

FIG. 4. Magnitude-vs-frequency distributions $\mathcal{D}(\mu)$, as shown in Fig. 3, scaled here so that the distributions of localized events coincide. The appropriate scalings presented here and in Fig. 5 are deduced from the conservation law (4.1), the scaling form suggested in (4.4) and continuity of this distribution at $\tilde{M}$, the dominance of the large events in displacing the system, and the numerical observations that the statistics of large events is described by $b' = -1$ and the scaling $M^*/\tilde{M} \sim l$.

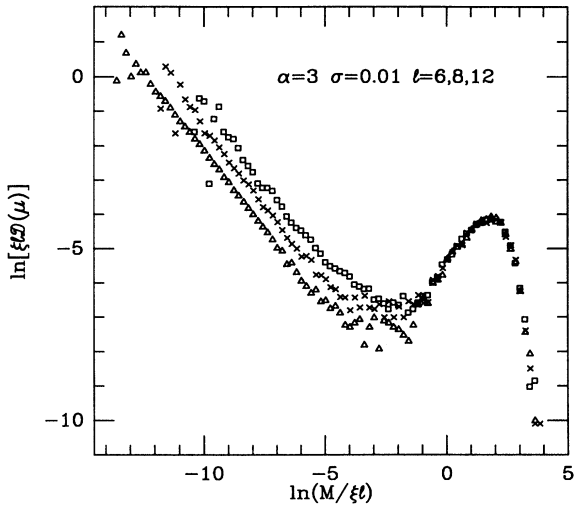

FIG. 5. Magnitude-vs-frequency distributions $\mathcal{D}(\mu)$, as shown in Fig. 3, scaled here so that the distributions of delocalized events coincide. Note that the scaling here is substantially different from that used in Fig. 4. The difference follows from the fact that delocalization crossover $\tilde{M}$ and upper cutoff M^* scale differently with l.

M^*, our numerical results indicate that the appropriate scaling is $M^*/\tilde{M} \sim l$, yielding a range of about two decades for realistic parameters:

$$\delta\mu_0 = \log_{10}\left[\frac{M^*}{\tilde{M}}\right] \sim \log_{10}(l) \approx 2 \ . \tag{4.8}$$

Therefore, if the smallest seismic event [8] is approximately of magnitude zero, then the model would suggest that the crossover between localized and delocalized events would roughly coincide with magnitude six, and the largest event would be roughly magnitude eight, which are of the right order seismologically.

As in Ref. [2], we observe significantly different behavior for sufficiently small values of α. Of course, the criterion for smallness of α is σ dependent. For $\sigma = 0.01$ and $\alpha = 1$, the sharp distinction between localized and delocalized events disappears, and we find that the distribution $\mathcal{D}(\mu)$ becomes well approximated by a single power law of the form

$$\mathcal{D}(\mu) \approx \frac{1-b}{M^*}\left[\frac{M^*}{M}\right]^b \quad (M < M^*) \ . \tag{4.9}$$

Here for the entire range of magnitudes there is a single scaling given by $M^* \sim \tilde{M} l^\gamma \sim \xi l^\gamma$, and b is strongly α dependent. In Fig. 6 we plot $\ln(\xi l^\gamma D)$ as a function of $\ln(M/\xi l^\gamma)$ for $\alpha = 1$, $\sigma = 0.01$, and $l = 6$, 10, and 14. The distributions lie on top of one another for the choice $\gamma = 0.65$. (Once again, the power-law dependence on l is meant simply as a rough description of our limited observations.)

We have also used the frequency distributions to make a direct check of the formula (3.6) for the localization length $\tilde{\xi}$. To do this, we plot the distribution $K(\Delta)$, which is the number of events per unit length of the fault

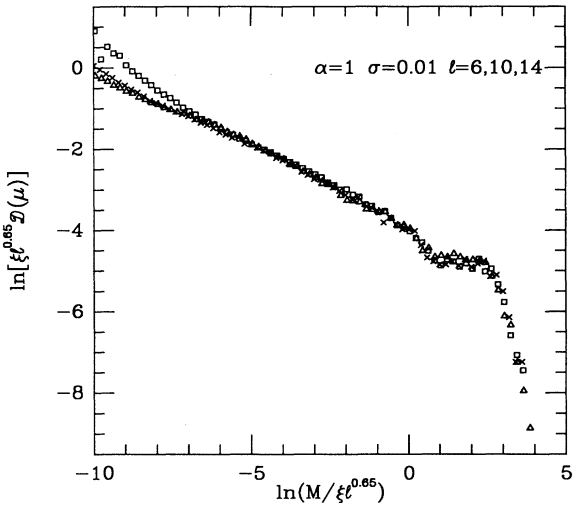

FIG. 6. Magnitude-vs-frequency distribution $\mathcal{D}(\mu)$ in the case of small α. Here, for $\alpha=1$, $\sigma=0.01$, and $l=6$ (squares), 10 (crosses), and 14 (triangles), we see that the distribution is described by a single power law with $b\approx 0.35$. Hence a single scaling suffices to collapse the distributions for different values of l onto a single curve.

and per unit average displacement as a function of Δ, the number of "blocks" that take part in the event [see Fig. 7(a)]. Note that, compared to $\mathcal{D}(\mu)$, which is well characterized by a pair of power laws describing the localized and delocalized events as in (4.4), $K(\Delta)$ seems to have more structure. It has a shallow minimum near $\Delta\approx\tilde{\xi}$, which we believe corresponds to the minimum of $\mathcal{D}(\mu)$, and thus locates the crossover between localized and delocalized events. We expect that the slight bend at $\ln(\Delta)\approx 2$, which coincides roughly with $\Delta=l$, may mark the crossover from the smallest microscopic events, in which the velocities scale with σ [as in (3.1)], and the larger but localized events, in which the velocities are independent of σ. In $K(\Delta)$, neither the localized nor the delocalized events seem to be well described by a single power law.

In Fig. 7(b) we compare the calculated value of $\tilde{\xi}/a$ with the value Δ_{cross} of Δ at the minimum $K(\Delta)$. Comparing data for a wide range of l, σ, and α, where α is sufficiently large that there is a definite distinction between localized and delocalized events, we find that typically (3.6) underestimates Δ_{cross}. Three effects contribute to this underestimate. First, we ignore the additional distance over which the velocity pulses decay as they leave the triggering zone and enter the stuck region. Second, we ignore nonlinear effects in the friction. Third, in our calculation we assume that all of the blocks are exactly at threshold when the event begins. However, some of the blocks will almost certainly be slightly stuck, in which case energy must be supplied to bring these blocks to threshold. Consequently, the pulses must travel through a somewhat larger region comprised of slightly stuck blocks to gain the same amount of kinetic energy that would be obtained from traveling through a region comprised of blocks exactly at threshold. Another

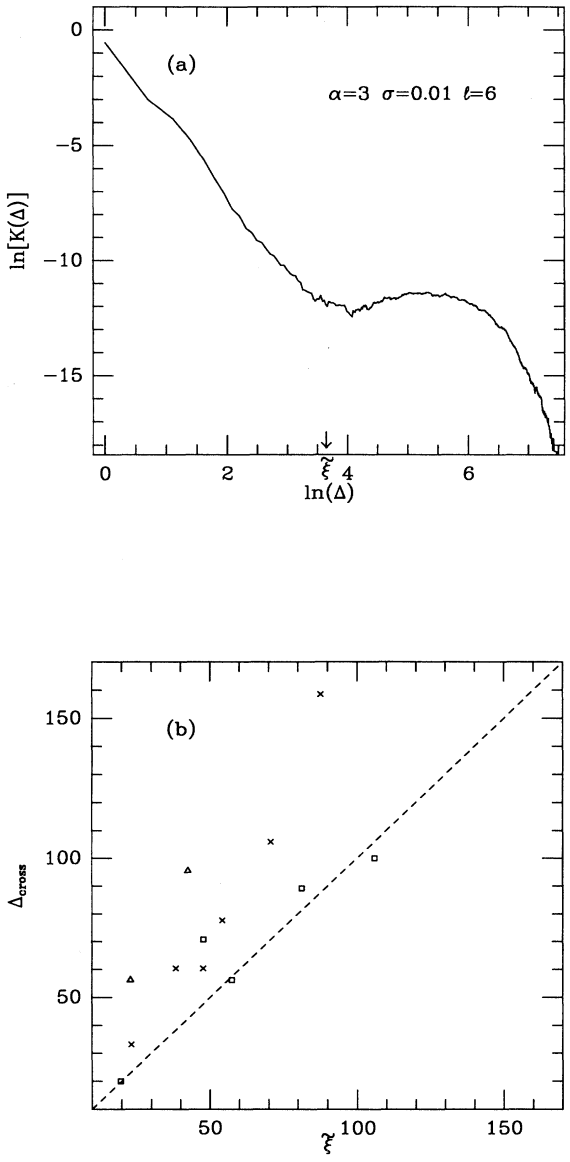

FIG. 7. To test our calculation of the transition length $\tilde{\xi}$ [Eq. (3.6)], we measure the slip-zone-size–vs–frequency distribution $K(\Delta)$, shown in panel (b) for $\alpha=3$, $\sigma=0.01$, $N=4096$, and $l=6$. The lower cutoff corresponds to one-block events, and the upper cutoff coincides with an event involving approximately 2000 blocks (over a period of roughly 400 loading cycles), which is significantly less than the system size. Note also that $K(\Delta)$ is not well described by a simple power law for either the localized or delocalized events. We identify the location of the local minimum of $K(\Delta)$ as $\Delta=\Delta_{\text{cross}}$, and compare Δ_{cross} with our calculated value of $\tilde{\xi}$. In panel (b) we plot Δ_{cross} vs $\tilde{\xi}$ for various values of l, σ, and $\alpha=2$ (squares), $\alpha=3$ (crosses), and $\alpha=5$ (triangles). While $\tilde{\xi}$ does provide a rough estimate Δ_{cross} (the dashed line $\Delta_{\text{cross}}=\tilde{\xi}$ indicates exact agreement), it typically underestimates the actual value. The variation of Δ_{cross} with l is consistent with (3.6) within our numerical accuracy (roughly, up to a power of l in the logarithm), though there seems to be a systematic shift in the fit as α is varied. A somewhat better fit is obtained by dropping the α dependence in (3.6); that is, by setting $\alpha=1$ in the formula.

feature that is apparent in Fig. 7(b) is the large amount of scatter in the data. This may be attributed at least in part to the ambiguity in determining Δ_{cross} from $K(\Delta)$, which is seen to have a relatively broad minimum without a sharp, well-defined crossover [note that $K(\Delta)$ is plotted on a logarithmic scale while Fig. 7(b) is not]. On the other hand, our results do indicate that the overall variation of Δ_{cross} as the parameters are varied is roughly consistent with our definition (3.6), supporting our calculation which indicates that $\tilde{\xi}$ sets the proper scale for the crossover.

V. RELATIONSHIP BETWEEN SOURCE PARAMETERS AND OBSERVABLE SIGNALS

The signals recorded by seismographs, conventionally reported as earthquake "magnitudes," do not generally have direct interpretations in terms of quantities one might hope to measure at the seismic source (the fault). Source parameters, in principle, correspond to a detailed description of the actual event—e.g., which parts of the fault moved, how far they moved, the duration of the event, and how much energy was released—and, therefore, knowledge of source parameters would be very useful for understanding earthquake dynamics, and possibly for predicting future events. In order to make a connection between the rupture source and the signal that arrives at the seismic station, a certain amount of modeling must be done. The results presented here for the model correspond to direct measurements of source parameters, while by obvious necessity the analogous seismic data is obtained indirectly from seismograms.

In addition to the net displacement between the plates, given by the seismic moment [13] M_0, there are several other source parameters which are of seismological interest. These include rupture area, earthquake duration, and energy release. As in the case of the seismic moment, certain assumptions are necessary to deduce these quantities from seismograms [14]. In this section we numerically determine the relations between these quantities in the model [15], and compare our results with the corresponding results in the seismological literature when available.

We begin with the earthquake duration τ_c, which is simply the time span of the rupture process. Typically, earthquakes last anywhere from tenths to hundreds of seconds. Certain anomalously "slow earthquakes" are also on record [16]. The duration of an earthquake is deduced from a seismogram by computing the Fourier transform of the seismic signal, referred to as the amplitude spectral density $\hat{u}(\omega)$. At small frequencies $|\hat{u}(\omega)|$ is approximately independent of ω, while at large frequencies $|\hat{u}(\omega)|$ bends over and decreases as a power of ω, roughly $|\hat{u}(\omega)| \propto \omega^{-\beta}$. These measurements are consistent with the model calculations of Haskell [17], which give $\beta=2$ for a unilaterally propagating fracture in which the moving front, i.e., the region that is slipping at any instant, is much narrower than the total rupture length. These calculations show that the duration τ_c of the event roughly coincides with the bend in the power spectrum, which is called the "corner frequency" (corner frequency $\sim 1/\tau_c$). The duration of an earthquake is related to the

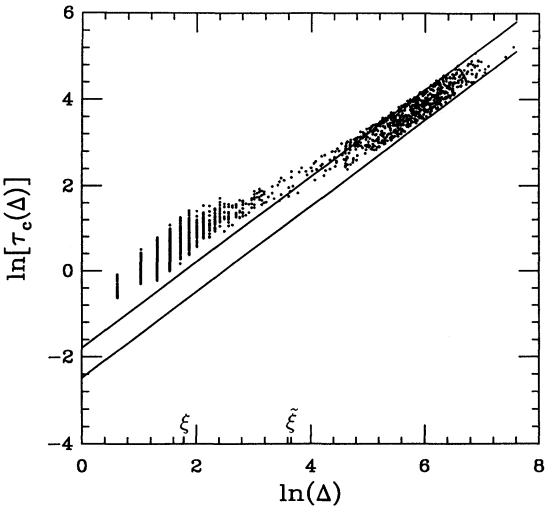

FIG. 8. Event duration τ_c vs slip-zone size Δ, shown here for $N=4096$, $l=6$, $\alpha=3$, and $\sigma=0.01$. The double-logarithmic plot illustrates that the range in durations for large events is consistent with our description of the events in terms of from one dominant (upper line) to two equal (lower line) pulses propagating out at the sound speed from an initial triggering point toward the boundary of the zone. The deviation for small events indicates that this simple description in terms of one or two propagating rupture pulses of a (roughly) fixed size breaks down. In this and the remaining figures, the individual data points corresponding to one-block events have been left off of the graphs.

length Δ_0 of the rupture zone by

$$c \approx \Delta_0/\tau_c \ , \tag{5.1}$$

where c is the rupture propagation speed, roughly 3 km/sec. The parameter ξ in our model is approximately equal to c in our units (recall that time is dimensionless, so ξ represents both a length and a velocity).

Figure 8 illustrates the results of the model. For the larger events, on average we find a linear relation with

$$\Delta/\tau_c \approx 3\xi/2 \ . \tag{5.2}$$

However, in Fig. 8 it is clear that there is a well-defined range of durations associated with events of a given size. Our numerical simulations show that the upper and lower bounds on the duration of the event grow linearly with the size of the slip zone, with

$$\xi \leq \Delta/\tau_c \leq 2\xi \tag{5.3}$$

for the largest events. Here the lower bound corresponds to the case in which the rupture propagates at speed ξ in just one direction, where the upper bound corresponds to the case of two pulses propagating in opposite directions, each traversing half of the total slip zone. Intermediate cases correspond to the triggering of the event somewhere in the middle of the zone, but not exactly at the center, so that two pulses are nucleated, but one is extinguished before the other. Interestingly, the smaller events deviate somewhat from this behavior, indicating that the simple description in terms of propagating pulses

is less applicable here. The small events last somewhat longer than would be expected from an extrapolation of the behavior of the larger events, and are better described in terms of a series of smaller, perhaps slower, pulses which may reflect several times from the stuck boundary back into the triggering zone before they die out. If this attribute was also characteristic of real earthquakes, a naive use of corner frequency would tend to overestimate the length of the slip region Δ_0 for small events.

For real data, measurements of the duration are used as an indirect way of estimating the rupture area A_0, which is determined from the corner frequency and Eq. (5.1), assuming a circularly symmetric rupture zone so that $A_0 \sim A_0^2$. Combining data from many different earthquakes, the scaling law

$$M_0 \sim \Delta_0^3 \sim A_0^{3/2} \tag{5.4}$$

is seen to hold reasonably well for a wide range of events (Δ_0 varies from meters to hundreds of kilometers), and is the basis for self-similarity assumptions in many models and predictive efforts [18]. In addition, when (5.4) is combined with certain theoretical assumptions, it implies that the stress drop along the displacement axis is independent of the magnitude of an earthquake. (Alternatively, the shear stress drop increases with magnitude, and is roughly proportional to Δ_0.)

In the model, for each slipping event, Δ is simply the number of blocks that move. In Fig. 9 we plot $M(\Delta)$ versus Δ for a sequence of events. Clearly, $M(\Delta)$ is not a simple power law in the model [19]. For the smallest (microscopic) events we find

$$M \sim \Delta^{3/2} . \tag{5.5}$$

This exponent agrees with our previous estimate [2] for microscopic events, in which we assumed a strictly uniform initial configuration in the slipping zone. With that assumption the event is triggered simultaneously throughout the zone, and blocks move in unison, stopping due to the increased compressional force at the boundary of the zone. This calculation yields very small displacements consistent with the scaling (5.5). A nonzero curvature $\partial^2 U/\partial s^2$ in the displacement in the zone will tend to increase the exponent. For example, a parabolic zone, $\partial^2 U/\partial s^2 = \text{const}$, leads to $M \propto \Delta^3$, a behavior which is not inconsistent with the intermediate behavior seen in Fig. 9. For the very largest events, it appears that

$$M \sim \Delta , \tag{5.6}$$

consistent with a description of large events that are dominated by highly energetic rupture pulses, which on average displace the system a constant amount as they move, stopping only when they encounter a region which is sufficiently firmly stuck. Thus, throughout the entire range of events, it is clear that M is not given by any single simple power of Δ.

The last source parameters that we will consider describe the energy transfer in the system. In particular, as a function of magnitude we individually measure the change in energy density due to changes in the longitudinal and shear stresses (in the language of the original Burridge-Knopoff model, the coupling springs and the pulling springs, respectively).

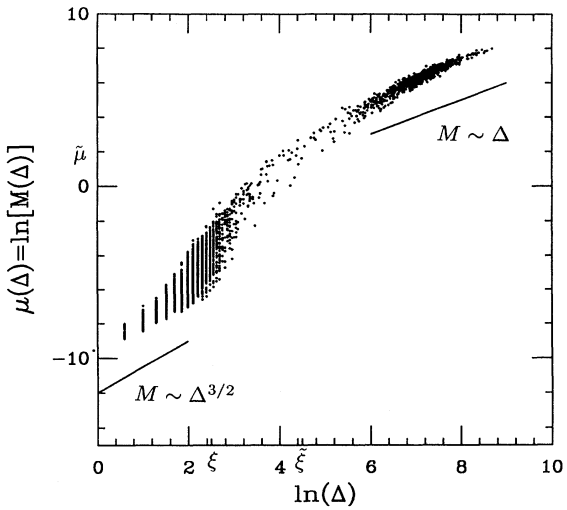

FIG. 9. Moment M vs slip-zone size Δ, shown here for $N=8192$, $l=12$, $\alpha=3$, and $\sigma=0.01$. Unlike earthquake data, in the model this curve is not well described by a single power law. The individual points represent individual events. Note that the distribution of moments for a given slip-zone size is relatively broad. The lines drawn below the points represent the asymptotic power-law behavior of the small and large events, as described in the text.

The change in the longitudinal elastic-energy density tells us which events are smoothing the system, and which events are roughening it. This is of particular importance for the model, where dynamic roughening plays a crucial role in generating future events. In the model, the longitudinal energy-density change is given by

$$E_L = \frac{1}{\Delta+1} \sum_{i\ \mathscr{E}} l^2[U_{i+1}(\tau+\tau_c) - U_i(\tau+\tau_c)]^2 - l^2[U_{i+1}(\tau) - U_i(\tau)]^2 , \tag{5.7}$$

where the event $\mathscr{E}$ lasts from time τ to $\tau+\tau_c$, and the sum is over the $\Delta+1$ coupling springs attached to the Δ slipping blocks. For real earthquakes, this is a very difficult quantity to measure, except perhaps on very large scales, although progress is being made at reconstructing local variations in the displacements during an earthquake [20].

Our results for the change in longitudinal elastic-energy density as a function of magnitude in the model are shown in Fig. 10, which illustrates our results both for individual events and on average. Note that for smaller events the average longitudinal-elastic-energy density decreases, indicating that these events primarily smooth the system, while this energy density increases only for the largest events, indicating a net roughening. As in the case of $M(\Delta)$, we see here that $E_L(\mu)$ has a great deal of interesting structure. The scatter in the data is largest for events of intermediate magnitudes, which are also the least frequent events. The smallest

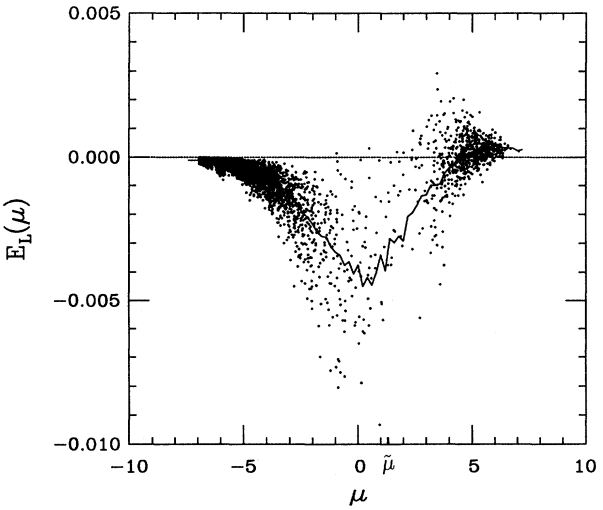

FIG. 10. Longitudinal elastic-energy-density change E_L vs magnitude μ, shown here for $N=4096$, $l=6$, $\alpha=3$, and $\sigma=0.01$. The points represent individual events, while the line drawn through them represents the average behavior (obtained from a much longer simulation than that associated with the individual points). The change in stored longitudinal (or "coupling spring") elastic-energy density is negative for small and moderate events, indicating a net smoothing, while for the largest events it is positive, indicating a net roughening. (The horizontal line $E_L=0$ distinguishes smoothing $E_L<0$ events from roughening $E_L>0$ ones.) Note that on average the maximum smoothing occurs near $\mu\approx\tilde{\mu}$; however, there is an enormous amount of scatter in the data, especially for the events of intermediate magnitudes.

events involving only one or a few blocks are very inefficient, resulting in only a very small net smoothing. As the size of the event increases, on average E_L decreases (net smoothing increases) monotonically until the magnitude reaches roughly $\tilde{\mu}$. At that point roughening beings to play a more important role, and on average $E_L(\mu)$ increases monotonically, becoming positive (net roughening) for very large events.

While the longitudinal stresses are well defined, there is some ambiguity in the absolute level of shear stress in both the model and the earth. In the earth, measurements focus mainly on stress drops associated with earthquakes. An estimate of the absolute stress level is given by the pressure as a function of depth, and under this assumption the absolute stress levels change relatively little in the earthquake cycle. In the model, the statement that stress drops are small compared to the absolute stress levels can be represented by a slipping friction which decreases by only a small amount relative to the sticking-friction threshold. However, in Eq. (2.1) the absolute stress level is ambiguous because adding a constant to the friction at high velocities can be viewed as simply shifting the zero of ϕ. The shift can be removed by redefining the zero of displacement or, equivalently, the zero of shear elastic energy, taking us back to the original dimensionless equation. Shear stress drops will thus be measured relative to the total change in force between the high-

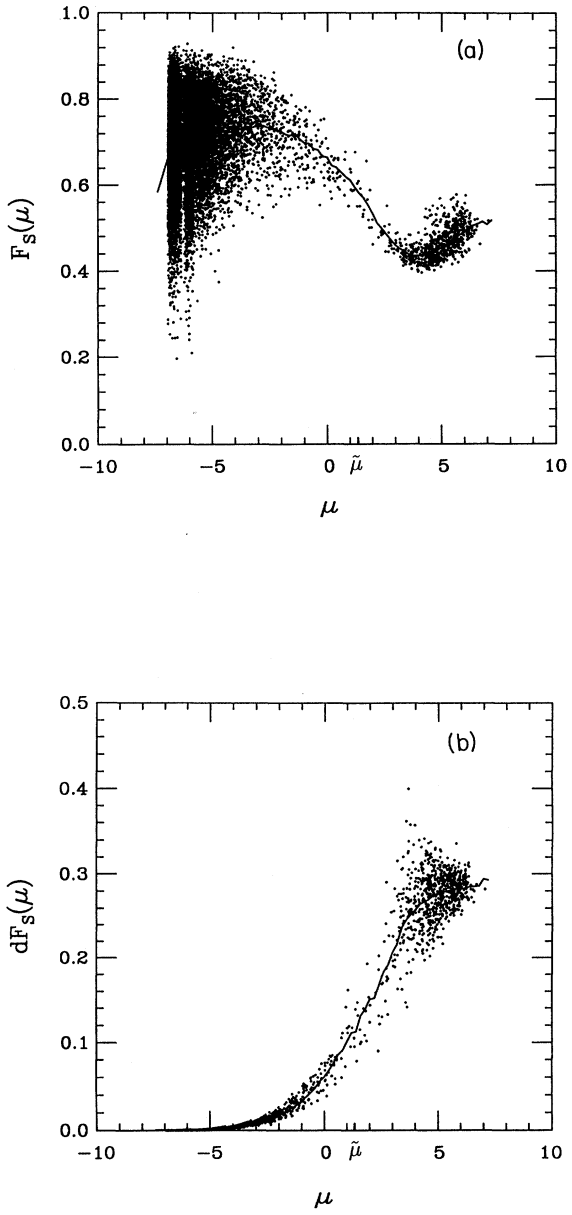

FIG. 11. Shear forces $F_S(\mu)$ and shear stress drops $dF_S(\mu)$ plotted as a function of magnitude μ, shown here for $N=4096$, $l=6$, $\alpha=3$, and $\sigma=0.01$. Panel (a) illustrates the average shear force F_S in the slip zone just before an event is triggered. As in Fig. 10, the dots represent individual events and the solid line shows the average behavior. For the small- and moderate-sized events on average the shear stress level is roughly 70% of its maximum value, indicating that the longitudinal stress contributes about 30% of the force necessary to trigger events. For the largest events, on average the shear stress level at the triggering time decreases, reflecting the fact that a significant fraction of the system which eventually slips may be far from threshold initially, but is nonetheless dislodged by the energetic rupture pulses propagating through the system. Panel (b) illustrates the average change in shear force in the slip zone for the same sequence of events. Comparing panels (a) and (b), it is clear that only the largest events relieve an appreciable fraction stored shear energy.

speed friction level (which is zero in our units) and the threshold (which is unity).

To determine the roles of the shear stresses for events, we calculate the average shear force in the slip zone just before an event begins:

$$F_S = \frac{1}{\Delta} \sum_{i \in \mathcal{E}} -U_i(\tau) , \tag{5.8}$$

where the event begins at time τ, and the sum is over the Δ blocks which will eventually slip in the event. The difference between the measured value and unity determines the role of longitudinal stresses. Our results, both for individual events and on average, are illustrated in Fig. 11(a). For the smallest events there is an enormous scatter in the data, reflecting the sensitivity of these events to local variations in the longitudinal stresses. However, on average, events of small and moderate sizes are triggered when the shear stress is approximately 70% of the maximum (this result is not strongly l dependent). A deviation from this result is seen for larger events, where the average shear stress at the triggering time reduces to roughly 40–50 % of the maximum value, which reflects the fact that, in large events, a significant fraction of the eventual slip zone is relatively far from threshold. Interestingly, $F_S(\mu)$ has a shallow minimum slightly above $\tilde{\mu}$, which may be clearly distinguished both for individual events and on average.

In Fig. 11(b) we plot the average change in shear force resulting from an event:

$$dF_S = \frac{1}{\Delta} \sum_{i \in \mathcal{E}} U_i(\tau+\tau_c) - U_i(\tau) , \tag{5.9}$$

where the sum is over the Δ blocks that slip in the event. Note that dF_S is simply the moment M divided by the slip-zone size Δ, and thus increases roughly exponentially as a function of magnitude [the increase would be strictly exponential if $M(\Delta)$ were a simple power law; see Fig. 9]. Comparing Fig. 11(b) to Fig. 11(a), we see that for the smaller events, an insignificant fraction of the shear stress is relieved. (Recall that when we speak of shear stress drops in the model, it is always relative to a maximum which is set by the difference between the threshold friction force and the friction force at high velocities.) Only for the largest events is the shear stress drop comparable to levels of stress when the event is triggered.

VI. CONCLUSIONS

In this paper we have presented a selection of statistical distributions which represent certain basic features of a deterministic, homogeneous, one-dimensional, Burridge-Knopoff model of a fault. We have also discussed the relationship between our results and the corresponding results for real faults. We summarize our principle findings below.

The intrinsic behavior of the model in principle is governed by just two dimensionless groups of parameters: the friction constant α and the triggering parameter σ (or the dimensionless pulling speed v, as used in Refs. [1] and [2]). In addition, there is a dimensionless stiffness constant which, in the finite-difference version of the equation of motion (2.2), is the number of mesh points in a stiffness length, and which therefore is supposed to become infinite in the continuum limit. Our analysis of the variation of the magnitude-versus-frequency distribution as the parameters are varied (Sec. IV) leads us to conclude that the finite size of l, i.e., the ultraviolet cutoff, plays an important role, even for the largest events. While we do not fully understand the mechanism, we expect that it may be a rather general consequence of stick-slip friction. This result should be kept in mind whenever a discretization scheme is used to study a system with a stick-slip instability; such models may not necessarily have well-defined continuum limits.

Our analysis of the magnitude-versus-frequency distributions also leads to explicit scaling relationships between three characteristic moments of events: the lower cutoff M_1, the upper cutoff M^*, and the moment $\tilde{M}$, at which there is a crossover between localized and delocalized events. When we substitute our rough estimates for the corresponding parameters for real faults into these equations, it is reassuring to note that our results are consistent with the observed ranges of real earthquakes.

In the model there is a sharp distinction between the smaller localized and larger delocalized events. The distinction is apparent both in the overall statistics, as in, for example, the magnitude-versus-frequency distributions of Sec. IV, and in the dynamics of individual events as seen, for example, in Sec. V, where we determine the relationships between various source parameters. For example, for large events our measurements of the event duration versus rupture-zone size are consistent with a description of the event in terms of one or two large rupture pulses traveling at the sound speed along the fault. In contrast, for the small events, our data are inconsistent with this picture. Instead, the smaller events are more likely to consist of a series of smaller pulses which reflect several times from the boundary of the slip zone before dying out. Another difference between small and large events is apparent in Fig. 10, where we plot the change in the longitudinal elastic-energy density as a function of magnitude: The small events primarily smooth the system, while the large events primarily roughen it. This has important implications for the magnitude-versus-frequency distribution of localized events, since it implies that these events are not self-generated, but rather comprise a relaxation process by which the chaotic configurations left after some prior large event are smoothed on smaller scales.

In the model, the magnitude-versus-frequency distribution is relatively simple, and can be well characterized by a pair of power laws describing the small and large events. In contrast, compared to magnitude (or moment), every other source parameter that we have measured gives rise to somewhat more complicated distribution. This suggests that moment might be a more universal measure of the behavior of the system. It also implies that attempts to understand the distribution of moments using a real-space renormalization may not be the best approach.

Because properties of small earthquakes are difficult to

measure, the extent to which many of these results are true for real earthquakes is still an open question. Even for the most robust feature of the model—the $b=1$ scaling in the magnitude-versus-frequency distribution of localized events—the corresponding value of b_0 for the distribution of seismic moments for small earthquakes remains an open seismological question. However, measurements that could help answer the question of the b_0 value for small events, while difficult, can now be made with current techniques used in seismology. We believe that the answer to this question is of fundamental importance, and urge that the effort be made.

ACKNOWLEDGMENTS

In the course of this work we have benefited from numerous useful discussions with C. Nicholson of the University of California at Santa Barbara (UCSB) Institute for Crustal Studies. Support was obtained from the U.S. Department of Energy under Grant No. DE-FG03-84ER45108 and the U.S. National Science Foundation under Grant No. PHY82-17853 at UCSB.

APPENDIX: FREQUENCY DISTRIBUTIONS FOR REAL EARTHQUAKES, AND A COMPARISON WITH RESULTS OBTAINED FOR THE MODEL

Our numerical simulations indicate that the distribution of localized events is well described by a power law: $D(M)\sim M^{-(b+1)}$, where $b\approx 1$, spanning many decades of moment M. The fact that this scaling persists for a wide range of system parameters is one of the most robust and interesting features of the model. However, because seismic measurements are indirect, a certain amount of modeling must be done in order to relate this result to analogous results obtained from seismograms—namely, the Gutenberg-Richter law. In this appendix we summarize various efforts which have been made in this direction.

Gutenberg and Richter [6] made the first series of systematic measurements leading to a statistical distribution of the number of earthquakes of a given size. They introduced a magnitude scale based on the logarithm of the maximum deflection of a seismographic needle, which responded to surface shear waves in a given fixed-frequency window. This original magnitude scale led to the development of a large number of related scales measuring different aspects of the radiation emitted by a seismic event. It is now generally recognized, however, that a scale based on properties of the source itself is the best measure of the size of an earthquake.

Both for the model and in the earth, there is a conservation law which states that over long periods of time displacement along a fault zone must match the relative motion of the tectonic plates as a whole. This suggests that for any individual earthquake the net displacement may be the best measure of the size of the event. In the model, this is the moment M, and in seismology this quantity is known as the "total moment." Unfortunately, it is not generally possible to measure directly the actual displacement along a fault except for the largest events. One must therefore use remote measures such as seismic radiation. The seismic moment M_0 is the closest measure of the total moment, and is obtained from the Fourier transform of a seismographic signal by extrapolating to the zero-frequency response of the instrument. It is generally assumed that the seismic moment is linearly related to the total moment, although this is not necessarily always the case [16].

Measurements of M_0 are most accurately obtained for large earthquakes. On the other hand, for small earthquakes, measuring M_0 is a difficult operation. Instead, seismologists typically measure the more easily obtained surface magnitude M_S [21], which measures the energy radiated via surface waves with a particular period of about 20 sec. The M_S scale is a generalization of the scale originally introduced by Gutenberg and Richter [22], and the number of events of size M_S is a well-known quantity. Worldwide data show

$$\log_{10}\mathcal{N}=A-bM_S\ , \tag{A1}$$

with $b=1$, $\mathcal{N}$ being the number of events with magnitude larger than M_S. This is the Gutenberg-Richter law. In order to obtain the corresponding relation for the seismic moment, empirical relations are needed to convert M_S to M_0. However, the conversion factor is not well known and is currently a topic of debate.

For a propagating crack embedded in a three-dimensional elastic medium, Kanamori and Anderson [14] calculated the radiation emitted at the frequencies at which the surface magnitude is measured. These calculations lead to the following theoretical formula relating M_S and M_0:

$$\log_{10}M_0\sim\begin{cases}M_S, & M_S<6\\ \frac{3}{2}M_S, & M_S>6\ .\end{cases} \tag{A2}$$

The crossover in the conversion factor at roughly magnitude six is associated with the crossover from events in which the duration is less than the inverse of the measurement frequency, to events in which the duration is greater. Ekstrom and Dziewonski [23] find empirical measurements consistent with this description [24]. However, there is by no means consensus on the issue. Wyss and Brune [25] find a conversion factor closer to $\frac{3}{2}$ in the range $3<M_S<6$, and Bakun [26] finds a continuously varying factor growing from around 1 for $M_S\sim 1$ events to around $\frac{3}{2}$ for $M_S\sim 4$. Thus it appears that the conversion factor is still an open question.

From this it is clear that a direct comparison between b values obtained from a model and those obtained empirically is rather tricky business. There is no direct measurement of total moment, the analog of our M, and the seismic moment M_0 is only obtained accurately for large events. Define the b_0 value for the seismic moment by $R_0(M_0)\sim M_0^{-(1+b_0)}$, where R_0 is the rate of events with moment between M_0 and M_0+dM_0. For the large events, when one averages over a regional fault system, a value of $b_0=\frac{2}{3}$ is observed, and is generally accepted. In contrast, there is no consensus on what the value of b_0 is for small earthquakes. To compare our results with

empirical data (i.e., M_S) for smaller events, we must rely on some conversion factor. If we use the conversion given by Eq. (A2) we obtain a b_0 value for the seismic moment given by

$$b_0 = \begin{cases} 1, & M_S < 6 \\ \frac{2}{3}, & M_S > 6 \end{cases} . \quad \text{(A3)}$$

For the small- and moderate-sized events, this result agrees with our model, which quite robustly generates the value $b = 1$ for a wide range of parameters. To obtain a value different from unity would require careful tuning of the friction parameter α—an unappealing prospect. While measuring seismic moments for small events is a difficult process, the techniques currently exist. We believe the value of b_0 for the small events is of fundamental importance, and is worthy of the effort that would be needed to resolve the question.

The model also indicates that there will be a statistical crossover at a magnitude corresponding to $\tilde{\mu}$. This crossover, and the corresponding length of the rupture zone $\tilde{\xi}$, can be estimated by setting the parameters in (3.6) equal to the approximate values for real earthquakes. Here ξ, the rupture propagation speed (a few km/sec) in units of the slipping time at a given point along the fault (seconds or less), is of order a few kilometers. As previously mentioned, $l = \xi/a$ is of order 10^2 if the smallest earthquake size a is of order tens of meters (the smallest scale a may be set by fault creep, and can vary). Assuming σ is not too small, the l dependence dominates the logarithm. Furthermore, as noted in Sec. II, we expect that the rate of the decrease of the slipping friction α is of order unity. This yields $\tilde{\xi}$ of order a few tens of kilometers. Because a magnitude six has a typical rupture length of roughly 10 km, the model gives a crossover scale which is consistent with Eq. (A3). It is important to emphasize, however, that the physical transition occurring in the model, between localized and delocalized events on a one-dimensional fault, may not be the same as the transition occurring in real earthquakes, between events that rupture less than the crust depth and events which rupture the crust depth. Thus the correspondence is far from clear.

The distribution of large events described in (A3) represents statistics compiled from a large collection of faults. Therefore, it lies somewhat outside the scope of the model, which represents a single fault. In the model, large events correspond to the "characteristic" earthquakes [27] of single faults—that is, the large events which are primarily responsible for the displacement of the fault. Statistics compiled from data on or near certain individual faults indicate that while Gutenberg-Richter statistics describe the distribution of smaller and moderate events, there is an excess associated with the largest events, as seen in the model. To describe the distribution of large events compiled from many faults it would be necessary to include a distribution of faults and fault lengths. Chen *et al.* [28] have proposed a model which generates a distribution of fault lengths consistent with the $\frac{2}{3}b_0$ value for large earthquakes.

[1] J. M. Carlson and J. S. Langer, Phys. Rev. Lett. **62**, 2632 (1989); also see P. Bak and C. Tang, J. Geophys. Res. **94**, 15 635 (1989); K. Ito and M. Matsuzaki, *ibid.* **95**, 6853 (1990); A. Sornette and D. Sornette, Europhys. Lett. **9**, 192 (1989).

[2] J. M. Carlson and J. S. Langer, Phys. Rev. A **40**, 6470 (1989).

[3] J. M. Carlson, J. Geophys. Res. **96**, 4255 (1991).

[4] B. Shaw, J. M. Carlson, and J. S. Langer, J. Geophys. Res. (to be published).

[5] R. Burridge and L. Knopoff, Bull. Seismol. Soc. Am. **57**, 341 (1967).

[6] B. Gutenberg and C. F. Richter, *Seismicity of the Earth and Related Phenomena* (Princeton University Press, Princeton, NJ, 1954).

[7] T. H. Heaton, Phys. Earth Planet. Inter. **64**, 1 (1990).

[8] P. E. Malin, S. N. Blakeslee, M. G. Alvarez, and A. J. Martin, Science **244**, 557 (1989).

[9] This localization condition is not unique. We expect that an alternative localization condition could be imposed by addressing more directly the dynamics of slipping pulses propagating through regions which are more firmly stuck. One would then ask when the pulses generated in the triggering zone are sufficiently large that they would not decay immediately upon leaving the triggering zone, but would rather propagate an appreciable distance into the neighboring regions. This condition will almost surely require displacements, which according to some criterion are sufficiently large at the end of the slip zone, thus producing a $\tilde{\xi}$ of roughly the form shown in (3.6), e.g., the prefactor $2\xi/\alpha$ will be unchanged since that arises from the growing pulses as they propagate through the triggering zone. However, a careful examination of the dynamics of the pulses could change certain factors in the logarithm, e.g., the power of l which appears.

[10] A similar effect has been observed in a related cellular automaton. See H. Nakanishi, Phys. Rev. A **41**, 7086 (1990).

[11] By "characteristic earthquake," we mean the large events have a typical size that is most often seen—the peak in the $\mathcal{R}(\mu)$ distribution. We do not mean to imply, as do some authors who use the term, that the distribution of slip along the rupture is identical for different large events.

[12] Our numerical simulations indicate that the slope of the distribution of large events has the value $-b' = 1$, as illustrated in Fig. 3. While this result is seen for a wide range of parameters in our simulations of Eq. (2.2), we expect that b' is not as universal as the b value characterizing the distribution of localized events ($b \approx 1$).

[13] We use the subscript 0 to denote the seismological quantities, as opposed to the nonsubscripted symbols that refer to our model. Our notation, however, is not fully consistent with the seismological conventions. See Appendix.

[14] H. Kanamori and D. L. Anderson, Bull. Seismol. Soc. Am. **65**, 1073 (1975).

[15] A similar set of measurements was made for an experimental system of blocks and springs in C. Y. King, Bull. Seismol. Soc. Am. **65**, 245 (1975).

[16] G. C. Beroza and T. H. Jordan, J. Geophys. Res. **95**, 2485

(1990).
[17] N. Haskell, Bull. Seismol. Soc. Am. **56**, 1811 (1964).
[18] The relationship $M \propto \Delta^3$ may not be as strong as is generally believed. There is a large scatter in the data, and there may be systematic deviations at very small earthquakes. For a typical plot of moment versus rupture size, see T. C. Hanks, Pure Appl. Geophys. **115**, 441 (1977). On the other hand, Shimazaki sees a difference in the scaling of the seismic moment for large and small events; K. Shimazaki in *Earthquake Source Mechanics,* American Geophysical Union Geophysics Monograph No. 37, edited by S. Das, J. Boatwright, and C. Scholz (AGU, Washington, DC, 1986), p. 209.
[19] For shorter systems in which large events tend to span the entire system, we find that the scaling $M \propto \Delta^3$ provides an excellent fit for the moderate to large events, and the only deviation is seen for the small events, where $M \propto \Delta^{3/2}$, as reported here.
[20] This is a continually evolving field. A standard text is K. Aki and P. G. Richards, *Quantitative Seismology* (Freeman, San Francisco, 1980).
[21] The seismological convention is to use the capital letter M, with different subscripts, to denote both the moment of an event and its magnitude.
[22] The local magnitude M_L, the original scale introduced by Gutenberg and Richter, is still used for the very smallest events.
[23] G. Ekstrom and A. M. Dziewonski, Nature (London) **332**, 319 (1988).
[24] This crossover magnitude is also associated with events in which the rupture spans the full depth of the crust; there is thus a change from qualitatively two-dimensional to one-dimensional ruptures at this magnitude.
[25] M. Wyss and J. N. Brune, J. Geophys. Res. **73**, 4681 (1968).
[26] W. H. Bakun, Bull. Seismol. Soc. Am. **74**, 439 (1984).
[27] S. G. Wesnousky, C. H. Scholz, K. Shimazaki, and T. Matsuda, J. Geophys. Res. **88**, 9331 (1983); S. Singh, M. Rodriguez, and L. Esteva, Bull. Seismol. Soc. Am. **73**, 1779 (1983); D. P. Schwartz and K. J. Coppersmith, J. Geophys. Res. **89**, 5681 (1984); F. C. Davison and C. H. Scholz, Bull. Seismol. Soc. Am. **75**, 1349 (1985).
[28] K. Chen, P. Bak, and S. P. Obukhov, Phys. Rev. A **43**, 625 (1991).